
Article:
Beagles, A., Fletcher, D. orcid.org/0000-0002-1562-4655, Peffers, M. et al. (2 more authors) (2016) Validation of a new model for railway overhead line dynamics. Proceedings of the ICE - Transport, 169 (5). pp. 339-349. ISSN 0965-092X

https://doi.org/10.1680/jtran.16.00020

Validation of a new model for railway overhead line dynamics

Adam Beagles[1] – PhD, MSc, BSc (Hons), Lecturer in Mechanical Engineering
David Fletcher[1] – PhD, BEng (Hons), Reader in Mechanical Engineering
Matthew Peffers[1] – MEng (Hons), AMIMechE, Graduate Engineer
Patric Mak[2] – PhD, BEng (Hons), CEng MIMechE, Senior Engineer (Systems & Software)
Caroline Lowe[2] – PhD, MSc, Bsc (Hons), CEng, Principal Engineer

[1]Department of Mechanical Engineering, University of Sheffield, UK
[2]Network Rail Infrastructure Limited, UK

Corresponding author: D.I.Fletcher@Sheffield.ac.uk

Abstract

This paper presents details of a new model of railway overhead electric power line dynamics for prediction of contact wire-pantograph contact forces and wire uplift. It is validated against data from EN50318:2002, and against data from track tests conducted at Network Rail's Melton Rail Innovation and Development Centre using a class 395 high speed electric multiple unit. Its advantage over previous approaches is its implantation in a commercial non-linear finite element package allowing application for a wide range of overhead line geometry.

Overhead electric lines and their support structures are highly stressed components largely without redundancy, and their integrity (both mechanical and electrical) is crucial to the functioning of railway infrastructure. Their failure can be understood in terms of component wear, fatigue and corrosion, in addition to electrical equipment life expiry. These processes are driven by a combination of factors including cable tension, dynamic load from current collection pantographs, the frequency of support, and environmental loading (e.g. sparking and sidewinds). The model described here is able to support decision making and cost effectiveness regarding these aspects for new installations (e.g. designing for compliance with EN50119:2009) and for maintenance of existing systems. The route for further extending its capabilities is outlined.

Keywords: Railway systems; Electrical engineering & distribution; Dynamics

List of notation

α	Mass proportional damping factor
β	Stiffness proportional damping factor
E	Young's Modulus
ν	Poisson's Ratio
σ	Standard deviation of the pantograph to contact wire force
c_0	Constant of integration
F_M	Arithmetic mean of the pantograph to contact wire force
T_0	Applied wire tension
w	Wire self-weight, assumed to be evenly distributed
x	Longitudinal direction, along the catenary,
y	Vertical direction, and catenary wire vertical profile
z	Lateral direction, across the track

1. Introduction

Overhead electric lines and their support structures are highly stressed components largely without redundancy, and their integrity (both mechanical and electrical) is crucial to the functioning of railway power supply infrastructure. Although overhead line systems are simple in concept, problems of poor dynamic behaviour and failures by wear and fatigue can develop affecting current collection quality and reducing the infrastructure lifespan. This paper describes the development and validation of a new model of dynamics of railway overhead line electrification equipment (OLE), to be applied as a decision support tool to assist in system design and maintenance.

Figure 1 shows an overview of a typical span of rail overhead power line. A tensioned contact wire is suspended, approximately parallel to the track beneath, from a catenary wire that is itself tensioned and supported by fixed masts. Electric trains are fitted with a pantograph that runs along the contact wire and current is drawn across the sliding contact between the two. In terms of mileage, just over a quarter of the UK rail network is currently electrified using 25kV AC OLE (Network Rail, 2009) with third rail DC electrification systems covering around 13%. Together, these account for almost 50% of train miles operated.

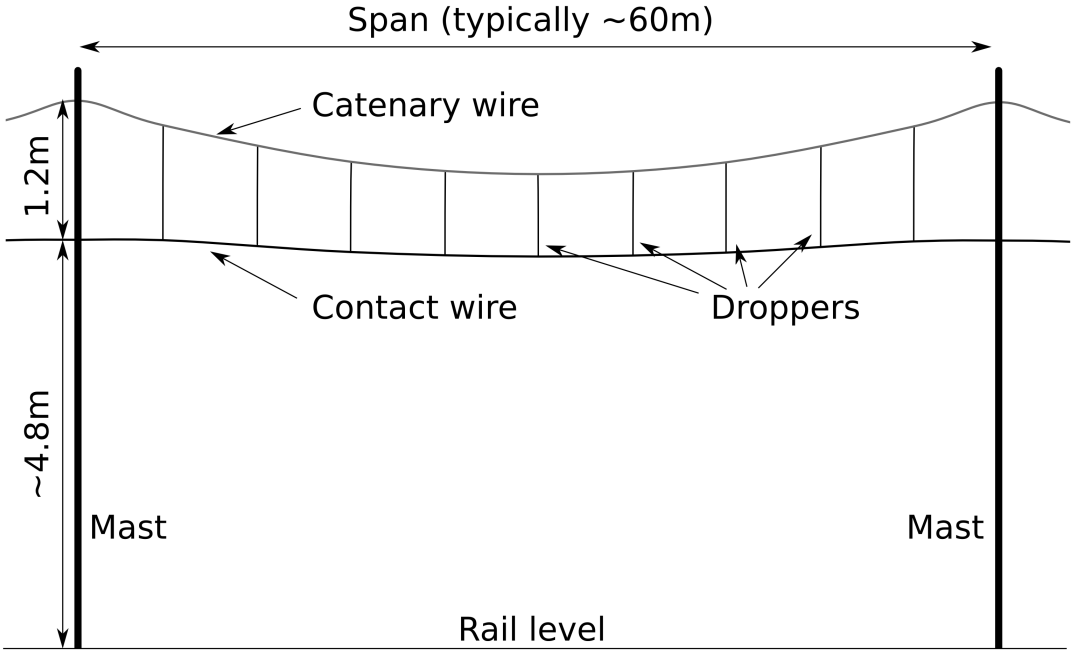

Figure 1. Two dimensional schematic representation of the overhead line system indicating key elements. Details of support, registration arms and stagger are excluded and dimensions indicate typical values.

1.1. Failure modes

Studies relating damage and failures in an OLE system to specific engineering changes made to the system include Shing and Wong (2008), but in most cases the information available is based on maintenance data from which it is less easy to establish the underlying cause of particular failures. Examining failures does however indicate two broad controlling issues: (i) Magnitude of uplift force on the contact wire from passing pantographs, and (ii) Cyclic application of uplift forces leading to fatigue cracking failures. The model developed here therefore focuses on predicting forces and uplift to drive a range of life prediction models, and failure modes are briefly reviewed to help in defining the information it needs to provide.

1.1.1. Contact Wire Wear

The sliding nature of the contact between the pantograph and the contact wire is conducive to wear of both surfaces. This is usually well-approximated by the Archard wear relationship (Williams, 1994) with proportionality between wear and the applied load, although the relationship can 'jump' between mild and severe levels of wear in cases where the system operates at significantly higher contact loads than designed. This would indicate that lower loads would be beneficial, however, loss of contact between the pantograph and contact wire can cause an electrical arc, rapidly raising the temperature of the surrounding contact wire (Auditeau et al., 2013). This can cause melting and vaporisation of the contact wire, effectively increasing the wear rate (Gonzalez et al., 2008). The model described here is able to make prediction of contact force to assist in finding a mid-range in which risk is reduced of both excessive sliding wear and loss of contact.

1.1.2. Contact Wire Fatigue

To ensure uninterrupted current collection, pantographs exert a force on the contact wire to maintain contact while in motion. This force acts to raise the compliant contact wire at the point of contact and causes a shear wave to travel forward in the contact wire (often referred to as a 'bow wave'. The prior displacement and deformation of the wire ahead of the pantograph will affect the resultant force between these components, but in addition this wave reflects off the different constituent parts of the catenary system, propagating further waves. This motion is only slowly damped away by the system after the passage of the train (Network Rail, 2014b). The cyclical loading of components can lead to fatigue failures, particularly at features in the overhead line where there is a change of stiffness (Network Rail, 2014b; Massat et al., 2011). Investigation requires quantification of the stress cycles present in the line.

1.1.3. Catenary Wire Fatigue

Catenary wires are also subject to fatigue failures. A particular problem has been noted in the UK with the catenary systems on the West Coast Main Line (WCML) and in East Anglia where the catenary wires pass over a pulley at each mast. These were intended to permit movement of the catenary wire as it expanded and contracted due to thermal effects, but have frequently resulted in wear, and in crack initiation, leading to fatigue failures (Taylor, 2013). Additionally, to reduce eddy losses in the catenary wire a braided cable is often used which can suffer failure through fretting damage between the individual strands as they move by different degrees as the wire bends (Lilien, 2013); this initiates and propagates cracks and the strands of the cable fail individually. As more strands break, the load-bearing cross-section of the catenary wire decreases, increasing the tensile stress in the remaining strands and leading to catenary failure if not detected. As with contact wire fatigue, understanding this process requires quantification of stress cycles in the catenary.

1.1.4. OLE Component Failures

The consequences of failure for some OLE components can be disproportionately serious. For example, if a dropper fails either at the interface with the messenger wire or part-way along its length, the broken section clamped to the contact wire is unsupported from above and can hang below the contact wire. From this position, there is a high risk of the broken dropper becoming entangled with a passing pantograph, causing significant damage to the pantograph and the surrounding OLE (Rail, 2013). Failures of other OLE components such as registration arms, porcelain insulators, and jumper wires are also commonly recorded during investigations of disruptions to rail transport involving OLE infrastructure (Robinson 2009). The root causes vary, but may include corrosion, fatigue, or overload caused by failure of other components, but again, quantification of forces and deflections during use or for a partially degraded system can assist in understanding and prevention of component failure.

1.2. Modelling approaches

The aim of the current work is to develop an easily-applicable, versatile, and maintainable model of the overhead line system. Initially this is to be validated on simple OLE spans, but with the capability for later extension to model features including neutral sections and bridge arms for limited clearance cases that are particular issues on the UK network. A variety of approaches to modelling an overhead line system exist and were reviewed to arrive at the decision to implement the new model in a commercial finite element analysis (FEA) system (ANSYS®, 2016).

The catenary system can be represented in a simple form by its spatial static stiffness variation (Wu and Brennan, 1998; Wu and Brennan, 1999), however, this simple representation does not allow satisfactory inclusion of components such as droppers or the phenomena of wave reflections in the system. An improved approach in which these can be represented is to model the contact and catenary wires as Euler-Bernoulli beams, with forces applied at discrete locations to simulate the dynamic boundary conditions; stiffness and damping properties of components such as droppers and registration arms can also be included (Bucca and Collina, 2007). The Euler-Bernoulli and Timoshenko beam methods are highly compatible with non-linear FEA, where the contact and catenary wires are discretised and the differential equations are solved for each individual section. Acceptable results can also be obtained using the modal analysis method, where the contact and catenary wires are decomposed into the sum of infinite derivable sinusoidal functions (Kia et al., 2010).

Gonzalez et al. (2008) used a computational modelling approach in their study on the wear rates of contact wires on the Metro de Madrid. A mass-spring-damper pantograph model featuring two lumped masses was passed under a catenary system with the wires represented by Euler-Bernoulli beams. The aim was to establish the implications for peak tensile stress in the contact wire of incorrectly installed under-length droppers, the added weight of splicing clamps (clamps used to connect spliced sections of contact wire from previous maintenance) and a localised area of high wear (and thus reduced cross-section) due to excessive arcing. A more complex computational study was undertaken by Pombo and Ambrósio (2013) concerned with current collection on high speed electric trains with two pantographs raised in response to environmental and track perturbations. A multi-body pantograph model and finite element Euler-Bernoulli beam catenary system were used in a co-simulation method. Each system functioned as an independent, standalone code but they were set to run in parallel and communicate. Also making use of Euler-Bernoulli beams to represent the catenary system, a model has been developed at Politecnico di Milano in conjunction with Italferr and Ferrovie dello Stato Italiane (Collina and Bruni, 2002). Pantographs were represented as lumped mass models, and the results were validated against data collected from the Italian rail network. Bucca and Collina (2007) have applied the model in conjunction with physical experimentation to predict the wear of both contact wires and pantograph collector strips.

Using the finite element method, SNCF have developed a pantograph-catenary dynamic simulation software called OSCAR (Outil de Simulation du CAptage pour la Reconnaissance de défauts) (Massat et al., 2011; Bobillot et al., 2006). This has been used in combination with real-time monitoring methods to give fast, location-specific, warnings about developing faults and OLE defects. Both lumped mass, with varying degrees of complexity (Avronsart, 2012), and multi-body pantograph models are supported (Bobillot et al., 2006). However, the closed source nature of the model means it did not fulfil the criteria of the current research aiming to develop a versatile and maintainable model able to target UK specific features of the overhead line infrastructure.

Following the review of existing models it was decided to proceed with a two-dimensional finite element based model, described in Section 2, which can later be extended to consider non-standard catenary layouts and overhead line components. In common with most other models it was decided to exclude (i) movement of overhead line mast foundations during the

passage of trains (the masts were taken to be fixed anchors for the wires), (ii) the effects of curved track layouts, (iii) the effects of sidewinds, and (iv) the lateral motion of the pantograph due to lateral train dynamics. It is planned to focus further development on (iii) and (iv), so the current model has been developed to support these extensions.

1.3. Model validation

Before developing the new model it was important to identify how it could be validated. Standard EN50318 (BSI, 2002) specifies a method for validating computational simulations of dynamic pantograph-catenary interaction. The recommended first stage is to benchmark the simulation against a reference model set out within the standard. Once a simulation is successfully validated against the reference model, second stage validation should be undertaken against alternative simulations or real line data collected in accordance with EN50317 (BSI, 2012), 'Requirements for and validation of measurements of dynamic interaction between pantograph and overhead contact line'. For the current model we have validated the simulation against real line data. It is recognised in the standard that the input parameters of the model must be varied between the first and second stages of validation, but that the modelling methodology must remain the same across both stages, and this was fulfilled in the validation of the current model.

1.3.1. EN50318 Reference model

The parameters to be compared between the EN50318 reference model and the simulation predictions are the arithmetic mean of contact force (F_M), the standard deviation of contact force (σ), the statistical minimum and maximum of contact force (defined as $F_M \pm 3\sigma$), the actual minimum and maximum of contact force, the maximum contact wire uplift at supports, and the percentage of loss of contact between the pantograph and the contact wire. For each of these quantities a range of acceptable values is defined for speeds of 250 and 300 km/h, and the results from the model, low-pass filtered at 20 Hz, must be within this range for the model to be regarded as valid (BSI, 2002).

The reference model from EN50318 defines a catenary system with a single contact wire, and consists of ten identical spans of 60m length, with encumbrance (height difference of contact and catenary wires at a support) of 1.2m. A stagger of ±0.2m is specified, however, since the model created here is a two-dimensional representation of the overhead line structure this is not incorporated. By modelling 10 spans the dynamic motion predicted over spans 5 and 6, for which statistical data are required, is intended to be stable and free of end effects.

The position of the droppers along each span for the reference model is defined in Table 1, taking the local mast position at the start of each span as the local origin. The dropper stiffness is defined as 100kN/m for tension and zero for compression. Catenary wire tension is set at 16kN, and contact wire tension at 20kN. These values are higher than those commonly used in the UK, but must be used to match the values in the reference model. The self-weight of the droppers and clamps is taken to be zero, with the mass of the wires defined as 1.07kg/m for the catenary, and 1.35kg/m for the contact wire.

Table 1. Dropper positions in validation model (BSI, 2002)

Dropper	1	2	3	4	5	6	7	8	9
Position / m	5	10.5	17.0	23.5	30.0	36.5	43.0	49.5	55.0

1.3.2. Data collected from real line tests

EN50318 validation requires fewer parameters to be assessed for data from track tests compared with the number for the reference model. This reflects the difficulty of collecting detailed data from real line testing. The parameters are (i) the standard deviation of the

contact force, (ii) the maximum uplift at the support, (iii) the range between the maximum and minimum vertical displacement of the point of contact. In all cases, a degree of accuracy of ±20% is required in the model outputs relative to the measured data (BSI, 2002).

Tests to generate real line data were undertaken at the Network Rail's Rail Innovation & Development Centre (RIDC) at Melton in the UK (formerly known as the Old Dalby test track (Network Rail, 2014a)), using a Hitachi Javelin (Class 395) train. The track is a former main line with a maximum gradient of 1:250, line speed available of up to 200km/h, and 18.5km of 25kV AC catenary. Use of the test track enabled more comprehensive monitoring of the overhead line and pantograph than would be possible on the mainline railway. However, the runs undertaken were part of a programme investigating overhead line faults such as missing droppers, different designs of neutral sections, and different pantograph designs (Bryan, 2014a; Bryan, 2014b). Variable span lengths and variable numbers of droppers per span were also part of the overhead line layout, giving a much more complex situation than would be found on many areas of mainline OLE. Overall, a 675m length of plain line at the RIDC was modelled, consisting of 12 spans with lengths ranging from 46 to 65m, each with 4 or 5 droppers, and with geometry defined to match that installed at the site (an example of the versatility achieved through the finite element package basis of the model). Catenary wire tension was 13kN, contact wire tension 16.5kN. Catenary wire cross sectional area was 65mm^2, and that for the contact wire 120mm^2. Testing for validation was undertaken at 185km/h.

2. Development of a new model

A two dimensional script based finite element representation of the overhead line was developed, with calculations performed using ANSYS version 14.5.7 on an Intel i7 based laptop computer. The procedure followed a sequence enabling the pre-tensions and self-weight of the catenary system to be created and balanced before application of dynamic loads from passing pantographs. Use of a script-based model allows the simple creation of a number of similar spans of catenary suitable for investigation of contact wire uplift and wire-pantograph forces, these being the key drivers of the failure mechanisms discussed in Section 1. Manual intervention is required only for special arrangements such as conductor bar in a tunnel, or detailed component models for investigation of specific issues.

2.1. Element types to represent OLE

Six ANSYS element types were used in the simulation. Table 2 summarises the properties and the behaviours of those chosen to capture the overhead line system, with values specific to the track test simulations. Values used for the reference model validation are in Section 1.3.1, and element types used to represent the pantograph in Section 2.2.1. Rayleigh damping was selected to represent the damping of the overhead line system (friction in joints, friction within braided cables, air resistance) with parameters α and β of 0.0055/s and 0.011s used to represent the very low levels of mass-proportional and stiffness-proportional damping present in the system.

Table 2. Element types used to represent components of the OLE

Application and element type	**Properties set (for test track validation)**	**Notes**
Catenary and contact wires BEAM189 - three-node Timoshenko beam	<u>Contact wire</u> Young's Modulus, E = 117GPa Poisson's Ratio, ν = 0.33 Mass per unit length, 1.07kg/m <u>Catenary</u> Young's Modulus, E = 100GPa Poisson's Ratio, ν = 0.34 Mass per unit length, 0.6kg/m	The contact wire profile was approximated as a solid circular cross-section with area equal to the real contact wire. The catenary wire, ordinarily a braided cable, was approximated as a solid circular cross-section with equivalent cross-sectional area.

Droppers COMBIN39 - non-linear spring	Stiffness in tension = 1260kN/m.	Droppers support tension but not compression and this behaviour was correctly represented by the element. Material properties and cross-section data are not required.
Droppers, clamps, registration arms MASS21 - structural mass	Dropper = 0.093 kg/m Contact wire clamp = 0.15 kg Catenary wire clamp = 0.15 kg Registration arm = 0.924 kg	Material properties and cross-section data are not required as these are treated simply as mass additions to the catenary.

2.2. Modelling the pantograph

The pantograph was modelled in a two-dimensional format allowing vertical movement under the catenary and translation along the contact wire. For validation against the EN50318 reference model the pantograph is specified by the standard to be a simple mass-spring-damper system (Figure 2a), and does not attempt to capture specific features of particular models. Nonlinearities such as bumpstops and friction elements were not included. Aerodynamic forces are taken to be zero, and a constant force of 120N is applied to the articulation frame mass to provide the static uplift force.

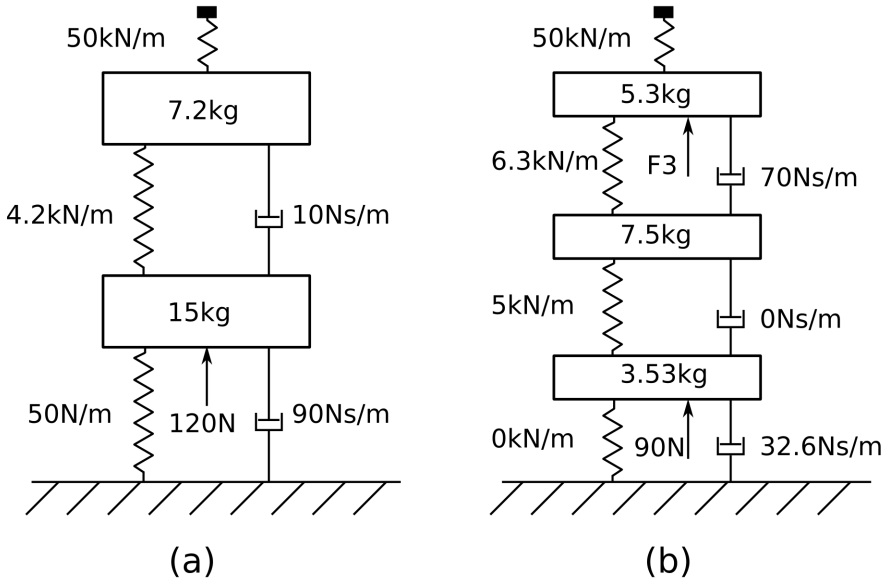

Figure 2. Mass, spring and damper representations of the pantograph. (a) Two mass version used in reference model validation. (b) Three mass version used for real line validation. Aerodynamic force F3 was given by velocity squared multiplied by a factor of 0.01301Ns²/m². The contact spring has a stiffness (k_c) of 50kN/m which is far above that of the other components and is required for contact modelling stability (BSI, 2002).

The capability to model both two- and three-lumped-mass pantographs was developed to enable more accurate representation of real pantographs with the mass, stiffness, damping, static and aerodynamic uplift forces fully defined. For validation against the real line track test work a three mass version was used (Figure 2b). The model has the capability to include more than one pantograph on a single train, but this capability has not been used in the results presented here. Since the pantograph is mounted on the vehicle body and above primary and secondary suspension the magnitude of any vibration at its base is typically much lower than the deflection of the wire (~40mm) under pantograph load, or the typical wire

height variation of around 2m that a pantograph can accommodate. As specified by EN50318 the base of the pantograph is taken to move smoothly with the train (shown as a fixed reference surface in Figure 2). Extension to consider side winds would require lateral movement of the train body and hence of the pantograph to be considered.

2.2.1. Elements used in the pantograph

Pantograph spring-dampers were represented using COMBIN14 linear spring-damper elements, and masses using MASS21 structural mass elements. The physical structure of the pantograph collector strips was represented by BEAM189 three-node Timoshenko beam elements, with elastic properties set to represent typical carbon collector strip (elastic deformation of the strip is not of interest in the model so these values are not crucial). The junction between the contact wire and pantograph is represented by CONTA176 and TARGE170 elements which are 3D line-to-line contact and target segment elements, and are overlaid on the wire and pantograph surfaces where contact is expected. Key options are set to define use of a penalty function contact algorithm for crossing beams. These element types are efficient for capturing global deflections and total force between the members that are of interest here, but would not be capable of examining the detail of pressure distributions at the interface if this were of interest.

2.3. Modelling workflow

Prior to the main modelling stages the overhead line geometry must be defined taking into account factors such as designed pre-sag of the spans, any differences in height between masts, and factors such as the extension of droppers under the weight of the contact wire they support. As OLE geometry measurements are typically only taken at the mast points, the full geometry is unlikely to be known. However, a good approximation can be obtained using the catenary curve (Eq. 1) which gives the vertical profile, y, of a wire as a function of its self-weight, w, (assumed to be evenly distributed) and the applied tension, T_0, with a constant of integration, c_0. As the catenary wire also supports the weight of the contact wire through the droppers, the self-weights of both wires must be included. Account can also be taken of any variation of height between adjacent masts by superposing a linear variation of height onto the standard catenary profile which assumes equal height masts. For each span, the x and y co-ordinates of the catenary wire at the two mast points are known, allowing the unknown c_0 to be eliminated.

$$y = \frac{T_0}{w}\cosh\left(\frac{w}{T_0}\cdot x\right) + c_0 \qquad (1)$$

The geometry points identified are those of the catenary under tension and self-weight, so some preliminary equilibrium modelling is needed to define the unloaded lengths which will achieve this geometry. At this stage use is made of COMBIN14 linear spring-damper elements in series with the catenary BEAM189 elements in the section of wire between the first/last dropper in each span and its adjacent mast. The spring element is specified with an initial length smaller than its final intended length, imposing tension at the start of a simulation. The stiffness of the linear spring is matched to the elastic properties of the catenary wire that it is representing. Once final geometry and wire lengths are defined, modelling is completed in two stages as described below.

2.3.1. Static wire equilibrium and boundary conditions

In the first modelling stage tensions and gravity are applied to the OLE components to pull them into their intended geometry. Pantograph/s are created at the start of the OLE with the collector heads positioned slightly below the contact wire enabling the wire to reach equilibrium before the pantograph load is applied. The desired result is the static equilibrium of the catenary so time integration is turned off. Global constraints are applied throughout the model to ensure that no components experience *z* (lateral) displacements and that there is no

rotation about the *x* (longitudinal) and *y* (vertical) axes. Global acceleration equal to gravitational acceleration applied in the y-direction to all nodes.

The catenary wire is constrained against displacements in all directions at its first point. It is constrained against y-direction displacements at all the mast points to replicate the support the masts give. No constraint in the x-direction is applied as this would prevent vibration transmission between spans in the catenary wire. Wire tension is applied in the x-direction at the end point. The contact wire is constrained against x-direction displacements at its first point. It is constrained against rotations about the z-axis at its first and last point to force the ends of the wire to approximate a continuous wire. Contact wire tension is applied in the x-direction at the end point. The mesh used 500mm-long Timoshenko beam elements on catenary and contact wires. Registration arms that provide lateral restraint (not represented in a two dimensional model) are included as mass additions to the contact wire (see Table 2).

The pantograph components are constrained against rotations about the z-axis. This keeps the pantograph entirely upright so all forces and displacements occur only vertically. The bottom is constrained against vertical (y-axis) displacements, i.e. the motion of the train on its suspension is not being considered. At this stage the collector head is constrained against y-direction displacements. While the cable tensions are being applied this helps close the initial gap between the collector head and contact wire in a controlled manner. The natural sag of the contact wire brings the two components into contact without the pantograph collector head rising at the same time due to the applied uplift forces. It also reduces the initial contact force and pantograph uplift prior to the start of the dynamic interaction load step. Before the dynamic interaction load step the pantograph is constrained against longitudinal (x-axis) displacements which may have been induced by, for example, any gradient in the contact wire. Following this load step a stabilisation step is included to allow residual velocities and accelerations of the nodes incurred as the pre-sag profile is formed to be completely damped out prior to dynamic modelling.

2.3.2. Dynamic solution

This load step begins from the geometry produced by the static modelling step. Time integration effects are turned on and auto time-stepping is turned off to give a full transient analysis with constant sub-steps, giving a constant frequency of data acquisition throughout the load step. Rayleigh damping is applied globally. The duration of this load step is determined by the time at which the leading pantograph reaches the end of the contact wire. Velocity is applied to the pantograph nodes moving them along the line to represent a train passing along the wire, with rotational and vertical constraint of the base remaining as previously described.

2.3.3. Outputs

Outputs produced by the model focus on the contact force at the contact wire to pantograph interface, wire displacement, pantograph displacement, and any loss of contact between the wire and pantograph, which would be expected to lead to arcing. EN50318 (BSI, 2002) lists outputs required of a model for validation against the standard, including post-processing of the data to produce statistics on standard deviation of contact force, statistical distribution (histogram) of contact force, time history of vertical displacement of the wire at any specific point along the track, and time history of the vertical displacement of any point of the pantograph. The current model is able to fulfil all these output requirements.

To aid model convergence sub-steps of the simulation are kept small resulting in data acquisition at a rate of 200Hz. The data was filtered using a Fast Fourier Transform followed by removal of high frequency components in the frequency domain. The remaining 0-20Hz data were converted back to the time domain, effectively performing a low pass filtering operation on the data. This frequency range is required for validation against the reference model (BSI, 2002), but a higher filter cut-off frequency could be used if high frequency

phenomena were of interest, for example, impact events around OLE fittings such as neutral sections.

3. Results and discussion

3.1. Reference model

For validation against the EN50318 reference model two runs were undertaken at pantograph (train) speeds of 250 km/h and 300 km/h. Although 10 spans were modelled the standard specifies that the section to be analysed is span 5 and 6 including their end supports. Data generated are listed in Table 3, showing that the newly developed model is able to achieve outputs within the expected ranges for all the elements specified by EN50318.

The statistical maximum of contact force for the 300km/h run is close to but within the maximum allowable. This may result from the new model having less damping than the comparators through use of shorter elements, or having less 'numerical damping' applied through the Rayleigh damping parameters to represent friction, for example at joints and within braided cables. The representation of the registration arm as a lumped mass on the contact wire rather than the pivoted mass of the real component would affect inertia, and lack of joints/friction would also change damping relative to the real component. The pantograph models were identical for the reference and new model so cannot account for any differences in behaviour.

Table 3. Results for the EN50318 reference and newly developed model.

	250 km/h		300 km/h	
	EN50318 reference model	Model	EN50318 reference model	Model
Mean contact force, F_M (N)	110 – 120	115.0	110 – 120	115.7
Standard deviation of contact force, σ (N)	26 – 31	29.9	32 – 40	38.0
Statistical maximum of contact force (N)	190 – 210	204.6	210 – 230	229.7
Statistical minimum of contact force (N)	20 – 40	25.3	-5 – 20	1.7
Actual maximum of contact force (N)	175 – 210	187.8	190 – 225	207.0
Actual minimum of contact force (N)	50 – 75	52.7	30 – 55	33.9
Maximum uplift at support (mm)	48 – 55	50.6	55 – 65	59.3
Loss of contact (%)	0	0	0	0

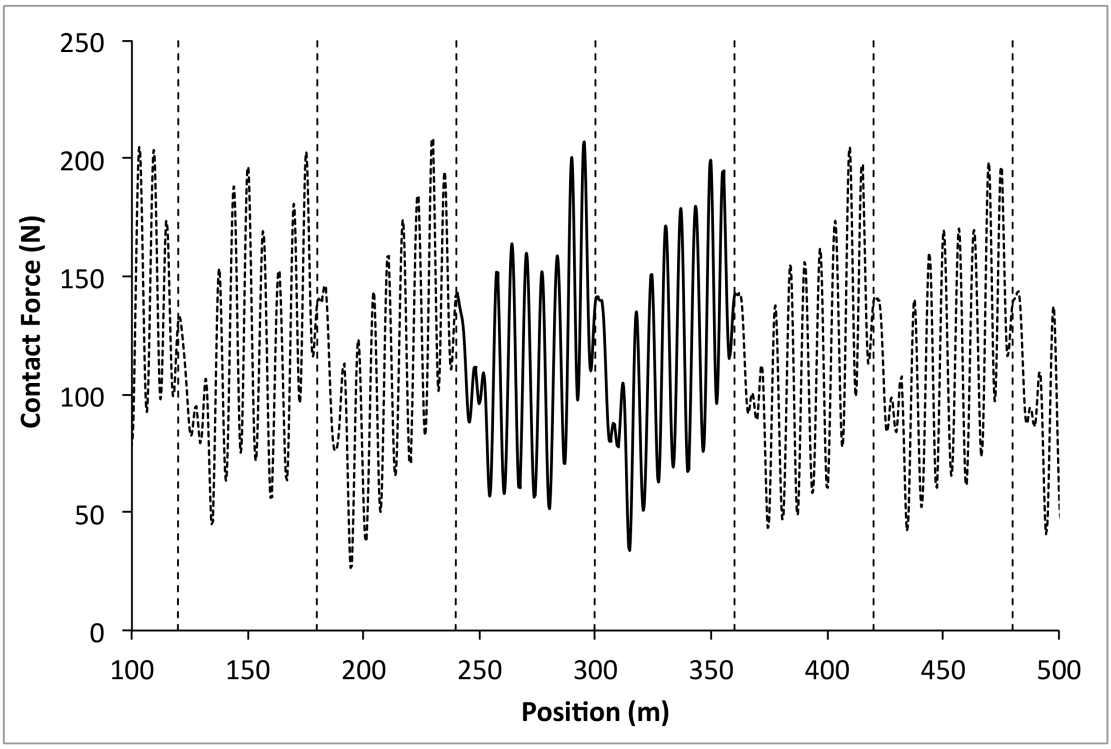

Figure 3. Variation of pantograph to contact wire force at 300km/h. Vertical chain lines are mast locations. Dotted line is the force data excluded from statistical analysis. Solid line is data for spans 5 and 6 which is used in statistical analysis. Pantograph moving left to right.

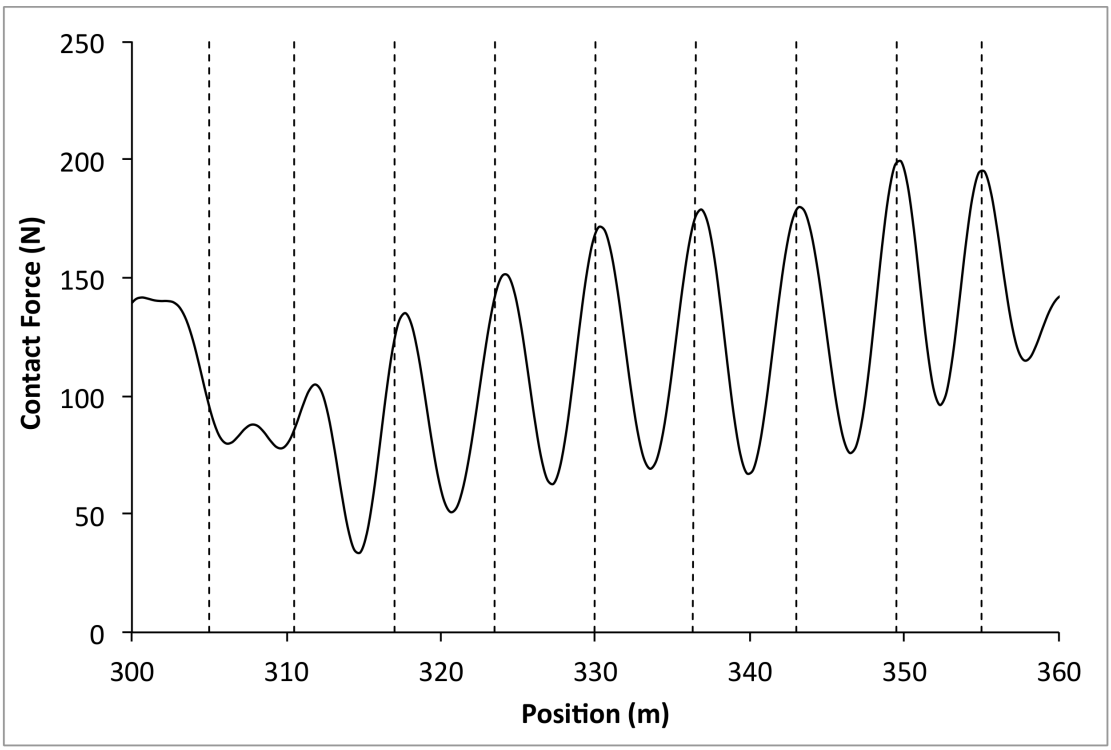

Figure 4. Detail of variation of pantograph to contact wire force in span 6 for the 300km/h run. Dotted lines indicate dropper locations. Pantograph moving left to right.

Plots of variation of pantograph to contact wire force with position are shown in Figure 3 and Figure 4. The saw-tooth pattern in the variation of pantograph to contact wire force during passage over multiple spans is also seen in results from OSCAR (Massat et al., 2011). It consists of two major frequency components: (i) a lower frequency envelope with a period set by the span length, and (ii) a higher frequency variation fixed primarily by the dropper locations, as indicated in Figure 4. Forces peak when passing droppers, or more exactly, just after passing droppers; this may at first appear to reflect the higher effective stiffness in these locations due to higher mass and consequent inertia, however, in the reference model the droppers and their clamps are implemented with zero mass so this is not the explanation. More important is the inertia of the pantograph (this inertia is both real and captured in the model). Moving along the contact wire the height of the wire varies, pushed up from its static position in which sag exists between droppers, particularly at the ends of the span where a larger length is unsupported (~10m, versus ~6m at mid-span, see Figure 1 and Table 1). The pantograph follows this height variation developing a force between itself and the conductor wire, and as the slope of the wire (i.e. rate of height variation) changes so does the force in proportion to the vertical acceleration. Figure 5 indicates the difference in slope of the contact wire ahead of the pantograph for contact positions at start, mid and end of span. The increasingly steep slope in the wire ahead of the pantograph as it moves through each span corresponding to the rise in force seen in Figure 3.

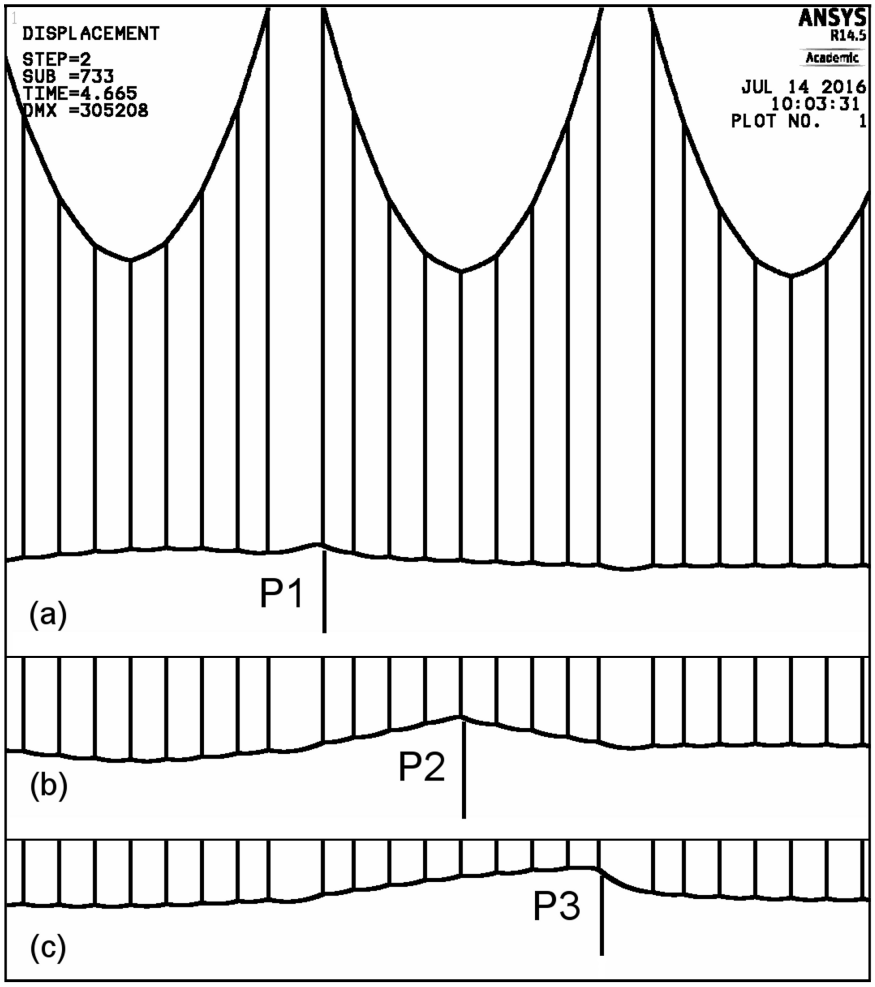

Figure 5. Reference model at 300km/h showing deformation of the contact wire local to the pantograph. (a) Pantograph at location P1, start of span. (b) Pantograph at location P2, mid-span. (c) Pantograph at location P3, end of span. Only the contact wire and droppers are shown in (b) and (c), but are aligned with the catenary shown in (a). Same scale in each section.

The variation in contact wire position over time at a single location is shown in Figure 6 and Figure 7 for train speeds of 300 and 250 km/h respectively. The predicted motion is for the mast at 240m which is at the start of span 5 and well within the stable running area of the model, away from 'end' effects such as running the pantograph up to speed at the beginning of the simulation. It can be seen that vertical oscillation of the contact wire begins well ahead of the passage of the pantograph, when the pantograph is still multiple spans along the OLE prior to the location considered. For a simple wire (without considering the supports, droppers, etc.) the speed of shear wave propagation can be found from the square root of the ratio of wire tension to the mass per unit length (Blevins, 2015). For the contact wire of the reference model this gives a wave propagation speed of 121ms^{-1}, i.e. well ahead of the pantograph speed of 300km/h (or 83ms^{-1}), so it is reasonable that motion of the contact wire begins ahead of the pantograph in this case.

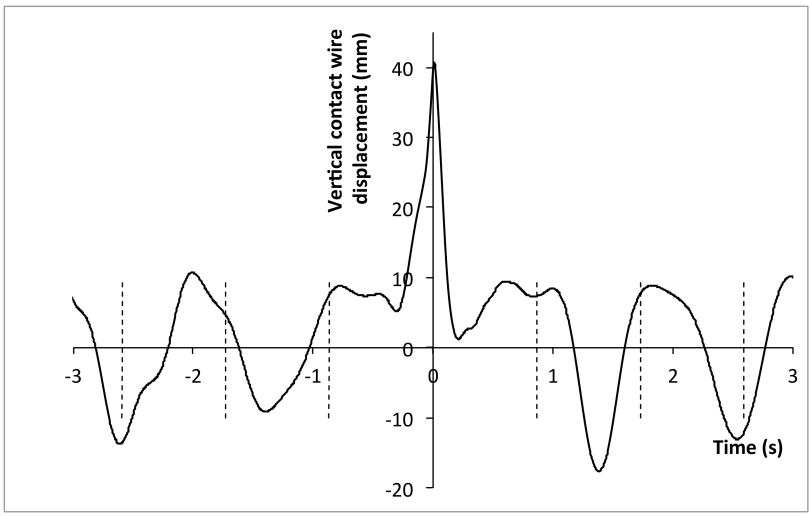

Figure 6. Variation of contact wire height at the mast at position 240m (start of span 5) for a 250km/h train. Origin of time is set to the point at which the pantograph passes the mast, i.e. negative time is movement of the wire before the pantograph arrives. Dotted lines indicate times of passing adjacent masts.

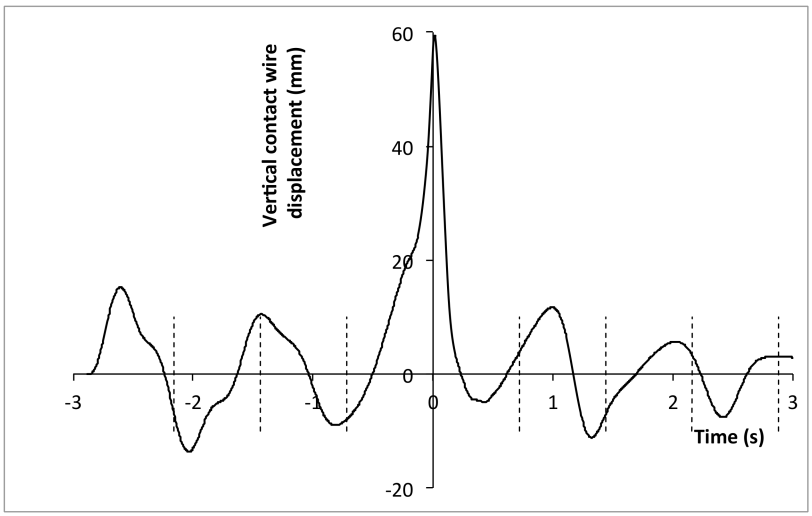

Figure 7. Variation of contact wire height at the mast at position 240m (start of span 5) for a 300km/h train. Origin of time is set to the point at which the pantograph passes the mast, i.e. negative time is movement of the wire before the pantograph arrives. Dotted lines indicate times of passing adjacent masts.

3.2. Validation with real line data

Table 4 indicates the results of the model and the test track data with a ±20% band for the parameters required for validation by EN50318. Spans five through to eight, at the centre of the 12 spans modelled were selected for analysis to avoid the initial settling of the model and end effects from influencing the results obtained. Note that the maximum uplift at the supports was not directly recorded during the test track work. Values for each of the five masts in the section corresponding to the modelling data were calculated from pantograph head height data, interpolated for each mast location. Except for the case of loss of contact between the pantograph and contact wire (which would in any case typically be a very small dynamic separation) this will accurately represent the position of the contact wire.

Table 4. Results for the track test data and newly developed model

	Track test data -20%	Model	Track test data +20%
Standard deviation of contact force, σ (N)	18.5	18.6	27.8
Maximum uplift at the support (mm)	37.4	40.7	56.1
Contact point vertical displacement range (mm)	56.6	61.2	84.9

The results obtained from the simulation for the three criteria listed in Table 4 were all within the range acceptable for EN50318 validation, although also all towards the lower end of that range, particularly in the case of the standard deviation of the contact force. This outcome is not unexpected as track data is subject to a wide range of noise factors not considered in the 'idealised' finite element model, most of which would be expected to increase variability of contact force. These will include the effect of track geometry and train dynamics on the base of the pantograph, whereas the model assumes the base of the pantograph to move linearly while remaining at a uniform height. Weather condition variation (wind, changes of temperature) were also present at the test track but not in the model. No attempt has been made here to optimise the pantograph model (Figure 2b) which may be another source of difference between the test track results and the modelling output. A useful future development of the model will be to include train dynamics, especially if lateral motion of the overhead line in side-wind were to be considered since lateral motion of the train under these conditions is also likely to be significant. However, the model achieves successful validation in its current form.

A fuller comparison of the model and track data can be made by looking at position based traces of contact wire-pantograph force (Figure 8) and pantograph height (Figure 9). The measured and simulated data show a good level of agreement, with the general trends and many of the peaks in the contact force traces replicated by the model. It is notable that the regular 'sawtooth' pattern present in the reference model case is not present when modelling real OLE geometry due to the more complex nature of the OLE geometry, although the reasoning behind the dependence of contact forces on wire angle and rate of height variation (Figure 5) remains relevant.

An important deviation between model and test data was in the second span in the analysed section in which the model predicted of a loss of contact event for track position 1505m that was not present in the measured test data. The origin of this event may be found in the data for pantograph head displacement at this track position that indicates the pantograph following a steep rise in wire height in both the model and track data. Here the pantograph needs to rise rapidly to maintain contact with the wire, and the prediction of contact loss at this point is not unreasonable given the train speed in this case was 185km/h. An improved representation of the pantograph dynamics in the model may be the route to removing this anomaly between the track and modelling data.

Looking at the histogram of contact wire to pantograph forces (Figure 10) shows a similar spread of values for each case, as would be expected given the similarity in standard deviation, Table 4. Viewing the data in this way focuses on the bulk of the data and avoids over-emphasising the outlying data points such as the loss of contact event discussed above. The modelling data shows a marginally lower mean contact force: mean 113.8N (track test) versus 104.7N (model), median 112.0N (track test) versus 103.3N (model). This sub 10N difference between the actual and predicted average forces represents very good agreement.

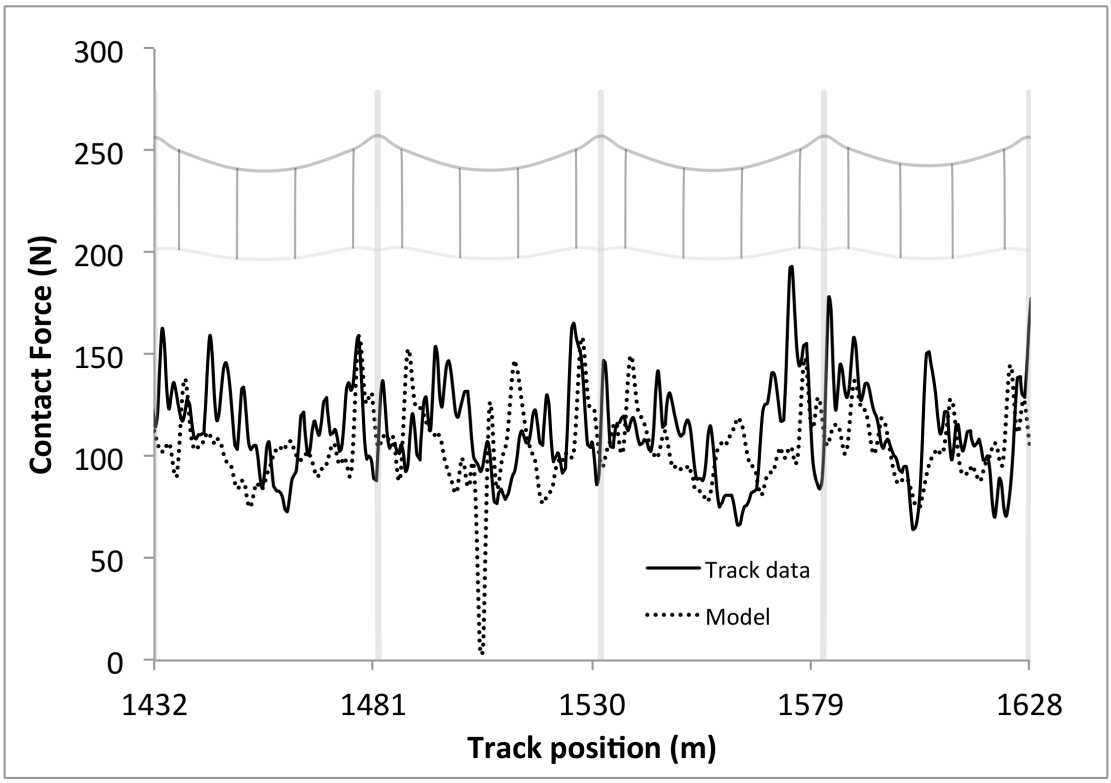

Figure 8. Data for contact wire to pantograph force, for model and test track. Background of the graph shows the overhead line layout in this region of the track.

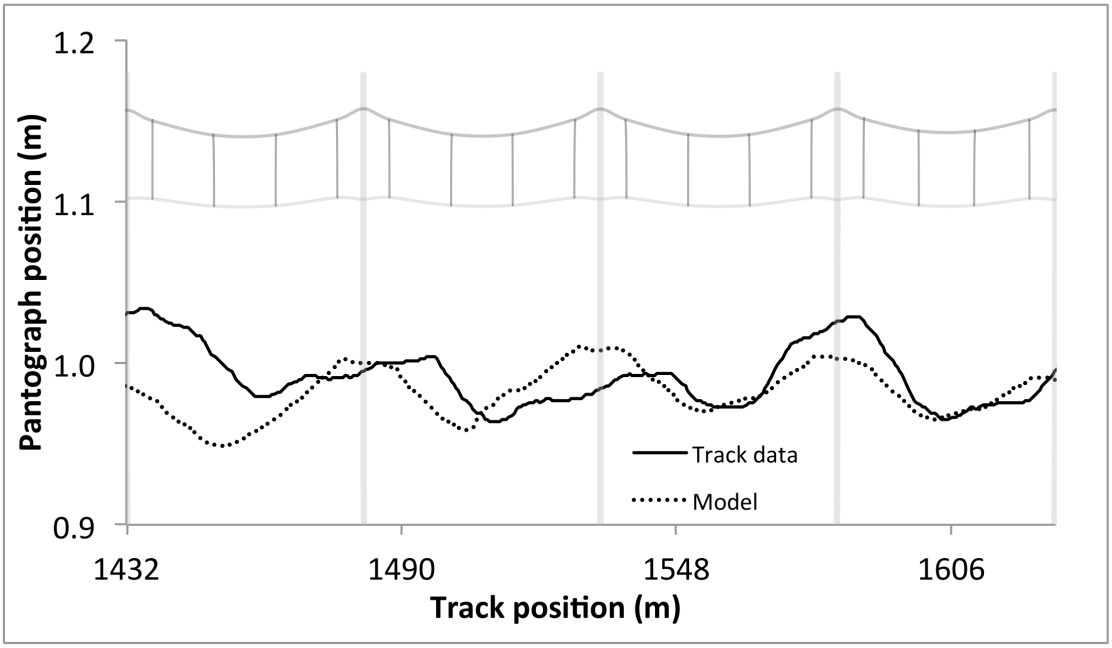

Figure 9. Data for pantograph head displacement, for model and test track. Background of the graph shows the overhead line layout in this region of the track.

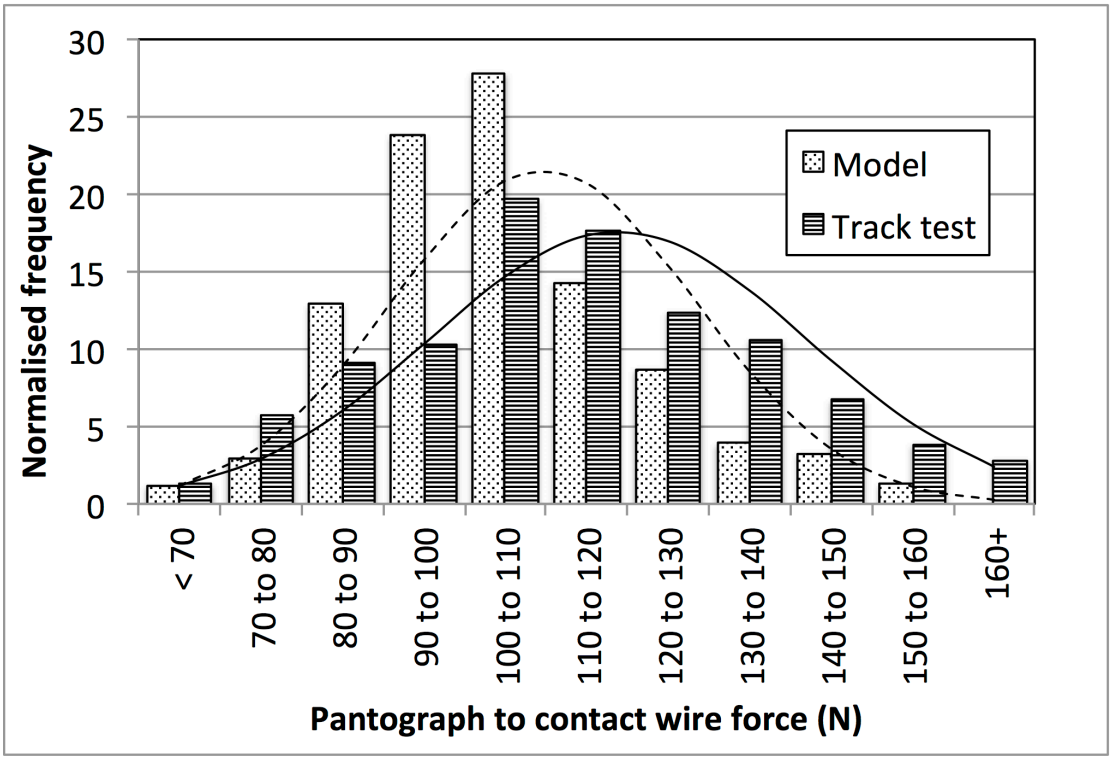

Figure 10. Histogram of contact wire to pantograph force data for real line tests and model predictions. Normal distributions are overlaid, using a dotted line for the model data. Normalised frequency indicates the percentage of data falling into each bin, thereby taking account of the different numbers of observations for the model and track cases.

4. Conclusions

A dynamic model of OLE equipment has been created using a finite element approach in ANSYS and the simulation method was successfully validated using the procedure outlined in standard EN50318. The model fulfils the requirement for an adaptable code that can readily be extended for specific OLE features of interest, for example to model the RIDC test track that included a wide range of OLE span and dropper spacing. Maintainability of the code is supported through its foundation in a widely used commercial finite element code designed for use by practising engineers, rather than in a computer language restricted to programmers. The outputs of the model may be applied in predicting overhead line life in respect of mechanical wear and fatigue failures, to support designing out these problems for new installations (e.g. while designing for compliance with EN50119:2009) and for maintenance of existing systems.

Validation of the OLE dynamic model against the reference model defined in EN50318 was successful, and this gave the confidence to undertake validation against real line data generated with a Class 395 high speed electric multiple unit at 185km/h. The real line data validation was successful, both statistically as required by EN50318 and in terms of absolute forces, with less than 10N difference in average contact force predicted by the model from that measured on track. Further development will focus on train dynamics and sidewinds, and on modelling specific OLE components including bridge arms and limited clearance cases of particular interest for electrification of existing non-electrified infrastructure.

5. Acknowledgements

The authors would like to thank Innovate UK, the Rail Safety and Standards Board, and Network Rail for co-funding the Knowledge Transfer Partnership (KTP № 9236) through which this work was undertaken. Thanks are due to Chris Bryan for his assistance in undertaking the test work, and for input of his valuable experience during the modelling. Testing was undertaken in conjunction with Hitachi, Brecknell Willis, and Serco, with drivers from Southeastern.

References

ANSYS® Mechanical Release 14.5 Help System (2016), ANSYS, Inc. http://www.ansys.com. (accessed 5th July 2016).

Auditeau G, Avronsart S, Courtois C, Krötz W (2013) Carbon contact strip materials -Testing of wear, Elektrische Bahnen **111(3)**: 186-195.

Avronsart S (2012) Optimising the interaction performance between pantograph and catenary for safe, secure and efficient transfer of energy, In *Cost Optimisation Electrification Infrastructure Congress*, available from http://www.cost-optimisation-electrification-congress.com/media/downloads/43-day-1-stephane-avronsart-sncf.pdf (accessed 6th July 2016).

Blevins RD, (2015) *Formulas for Dynamics, Acoustics and Vibration*, Wiley-Blackwell, Oxford, UK, ISBN-13: 978-1119038115.

Bobillot A, Delcourt V, Demanche P, and Massat JP (2006) Pantograph-Catenary: Three paths to knowledge, In *Proceedings of World Congress on Railway Research 2006*, available from http://www.uic.org/cdrom/2006/wcrr2006/pdf/210.pdf (accessed 6th July 2016).

BSI (2002) EN 50318:2002 Railway applications - Current collection systems - Validation of simulation of the dynamic interaction between pantograph and overhead contact line, British Standards Institute, London, UK.

BSI (2012) EN 50317:2012 Railway applications - Current collection systems - Requirements for and validation of measurements of the dynamic interaction between pantograph and overhead contact line, British Standards Institute, London, UK.

Bryan C (2014a) Overhead Line Dynamic Performance - Using statistical design to aid computer simulation of Series 1 equipment, Version 0.5, 21st January 2014, Network Rail, The Quadrant: MK, Elder Gate, Milton Keynes, MK9 1EN.

Bryan C (2014b) Series 1 Old Dalby Test Results - Data processing summary of Brecknell Willis Pantograph tests, Version 0.5, 17th September 2014. Network Rail, The Quadrant: MK, Elder Gate, Milton Keynes, MK9 1EN.

Bucca G and Collina A (2007) A procedure for the wear prediction of collector strip and contact wire in pantograph–catenary system, Wear **266(1-2)**: 46-59.

Collina A and Bruni S (2002) Numerical simulation of pantograph-overhead equipment interaction, Journal of Vehicle System Dynamics **38(4)**: 261-291.

Gonzalez FJ, Chover JA, Suárez B, and Vázquez M (2008) Dynamic analysis using finite elements to calculate the critical wear section of the contact wire in suburban railway overhead conductor rails, Proceedings of the IMechE, Journal of Rail and Rapid Transit **222(2)**: 145-157.

Kia, SH, Bartolini, F, Mpanda-Mabwe, A, Ceschi, R (2010) Pantograph-catenary interaction model comparison, In *Proceedings of the IECON 2010 - 36th Annual Conference on IEEE Industrial Electronics Society*, pp. 1584 – 1589. DOI:10.1109/IECON.2010.5675448.

Lilien J (2013) Power Line Aeolian Vibrations. Published by University of Liège Department of Electronics, Electricity and Computer Sciences, Liège, Belgium

Massat JP, Nguyen-Tajan TML, Maitournam, H, Balmès, E and Bobillot, A (2011) Fatigue analysis of catenary contact wires for high speed trains, In *Proceedings of the 9th World Congress on Railway Research*, http://www.railway-research.org/IMG/pdf/e3_massat_jean_pierre.pdf (accessed 6th July 2016).

Network Rail (2009) Route Utilisation Strategy, Electrification, October 2009, http://www.networkrail.co.uk, Network Rail, 1 Eversholt Street, London, NW1 2DN.

Network Rail (2014a), Rail Innovation and Development Centre (Melton and Tuxford), 9 May 2014, Network Rail, Milton Keynes, UK.

Network Rail (2014b) OLE Neutral Section Reliability Review - Final Report, INV-1-2102, 18th September 2014, Network Rail, Milton Keynes, UK.

Pombo J and Ambrósio J (2013) Environmental and track perturbations on multiple pantograph interaction with catenaries in high-speed trains, Computers and Structures **124**: 88-101, DOI:10.1016/j.compstruc.2013.01.015.

Rail (2013) East Coast Main Line suffers yet another massive failure. http://www.rail.co.uk/rail-news/ecml-suffers-another-failure/ (accessed 7th August 2014).

Robinson, P and Bryan, C (2009) Network Rail Electrical Power Reliability Study, Network Rail, Milton Keynes, UK.

Shing AWC and Wong PPL (2008) Wear of Pantograph Collector Strips. Proceedings of the IMechE, Journal of Rail and Rapid Transit **222(2)**: 169-176.

Williams J (1994) Engineering Tribology, Oxford University Press, Oxford, UK, ISBN 0198565038.

Taylor G (2013) A bad wire day. The Rail Engineer, 15th April 2013, http://www.therailengineer.com/2013/04/15/a-bad-wire-day/ (accessed 8 August 2014).

Wu TX and Brennan M (1998) Basic Analytical Study of Pantograph-Catenary System Dynamics, Journal of Vehicle System Dynamics **30(6)**: 443-456.

Wu TX and Brennan, M (1999) Dynamic stiffness of railway overhead wire systems and its effect on pantograph-catenary system dynamics, Journal of Sound and Vibration **219(3)**: 483–502.

Figure captions

Figure 1: Two dimensional schematic representation of the overhead line system indicating key elements. Details of support, registration arms and stagger are excluded and dimensions indicate typical values.

Figure 2: Mass, spring and damper representations of the pantograph. (a) Two mass version used in reference model validation. (b) Three mass version used for real line validation. Aerodynamic force F3 was given by velocity squared multiplied by a factor of 0.01301Ns²/m². The contact spring has a stiffness (k_c) of 50kN/m which is far above that of the other components and is required for contact modelling stability (BSI, 2002).

Figure 3: Variation of pantograph to contact wire force at 300km/h. Vertical chain lines are mast locations. Dotted line is the force data excluded from statistical analysis. Solid line is data for spans 5 and 6 which is used in statistical analysis. Pantograph moving left to right.

Figure 4: Detail of variation of pantograph to contact wire force in span 6 for the 300km/h run. Dotted lines indicate dropper locations. Pantograph moving left to right.

Figure 5: Reference model at 300km/h showing deformation of the contact wire local to the pantograph. (a) Pantograph at location P1, start of span. (b) Pantograph at location P2, mid-span. (c) Pantograph at location P3, end of span. Only the contact wire and droppers are shown in (b) and (c), but are aligned with the catenary shown in (a). Same scale in each section.

Figure 6: Variation of contact wire height at the mast at position 240m (start of span 5) for a 250km/h train. Origin of time is set to the point at which the pantograph passes the mast, i.e. negative time is movement of the wire before the pantograph arrives. Dotted lines indicate times of passing adjacent masts.

Figure 7: Variation of contact wire height at the mast at position 240m (start of span 5) for a 300km/h train. Origin of time is set to the point at which the pantograph passes the mast, i.e. negative time is movement of the wire before the pantograph arrives. Dotted lines indicate times of passing adjacent masts.

Figure 8: Data for contact wire to pantograph force, for model and test track. Background of the graph shows the overhead line layout in this region of the track.

Figure 9: Data for pantograph head displacement, for model and test track. Background of the graph shows the overhead line layout in this region of the track.

Figure 10: Histogram of contact wire to pantograph force data for real line tests and model predictions. Normal distributions are overlaid, using a dotted line for the model data. Normalised frequency indicates the percentage of data falling into each bin, thereby taking account of the different numbers of observations for the model and track cases.

Table captions